MCPyV Large T antigen induced atonal homolog 1 (ATOH1) is a lineage-dependency oncogene in Merkel cell carcinoma

Kaiji Fan[1,2,3,4], Jan Gravemeyer[1,2,3], Cathrin Ritter[1,2,3], Kashif Rasheed[5], Thilo Gambichler[6], Ugo Moens[5], Masahiro Shuda[7], David Schrama[8], and Jürgen C. Becker[1,2,3,9, §]

[1]Department of Translational Skin Cancer Research, University Hospital Essen, Essen, Germany
[2]German Cancer Consortium (DKTK), Partner Site Essen, Essen, Germany
[3]German Cancer Research Center (DKFZ), Heidelberg, Germany
[4]Department of Dermatology, Medical University of Graz, Graz, Austria
[5]Department of Medical Biology, University of Tromsø, Tromsø, Norway
[6]Department of Dermatology, Ruhr-Universität Bochum, Bochum, Germany
[7]Department of Microbiology and Molecular Genetics, University of Pittsburgh, Pittsburgh, United States
[8]Department of Dermatology, University Hospital Würzburg, Würzburg, Germany
[9]Department of Dermatology, University Hospital Essen, Essen, Germany

[§]to whom correspondence should be addressed: Jürgen C. Becker, Department of Translational Skin Cancer research, Universitätsstraße 1, S05 T05 B24, Essen 45141, Germany. Phone: +49 201-1836727, Email: j.becker@dkfz.de , Fax: +49 201-1836945

Running Title: ATOH1 in MCC

Keywords: ATOH1, miR-375, Neuroendocrine, MCPyV, LT

Abbreviations: ATOH1, atonal bHLH transcription factor 1; ASCL1, achaete-scute homolog 1; bHLH, basic helix-loop-helix; CK20, cytokeratin 20; DsiRNAs, Dicer-Substrate siRNA; LT, large tumor antigen; MCC, Merkel cell carcinoma; MCPyV, Merkel cell polyomavirus; sT, small tumor antigen.

ABSTRACT

Despite the fact that the transcription factor atonal homolog 1 (ATOH1) is a master regulator of Merkel cell development, its role in Merkel cell carcinoma (MCC) carcinogenesis remains controversial. Here, we provide several lines of evidence that ATOH1 is a lineage-dependency oncogene in MCC. Luciferase assays revealed binding of ATOH1 and subsequent activation to the promoter of miR-375, i.e. one of the most abundant microRNAs in MCCs. Overexpression of ATOH1 in variant MCC cell lines and fibroblasts induced miR-375 expression, whereas ATOH1 knockdown in classical MCC cell lines reduced miR-375 expression. Moreover, ATOH1 overexpression in these cells changed their growth characteristics from adherent to suspension/ spheroidal growth, *i.e.*, resembling the neuroendocrine growth pattern of classical MCC cell lines. Notably, ectopic expression of different Merkel cell polyomavirus (MCPyV) derived truncated large T antigens induced ATOH1 expression in fibroblasts, which was paralleled by miR-375 expression and similar morphologic changes. In summary, MCPyV associated carcinogenesis is likely to induce the characteristic neuroendocrine features of MCC via induction of ATOH1; thus, ATOH1 can be regarded as a lineage-dependency oncogene in MCC.

INTRODUCTION

Merkel cell carcinoma (MCC), *aka* neuroendocrine carcinoma of the skin, is a very aggressive cancer. It is less common as malignant melanoma, but its case fatality rate (33% *versus* 15%) is higher (Kaae et al., 2010, Stang et al., 2018). UV light exposure, advanced age, immune suppression as well as bearing hematological disorders such as B-cell chronic lymphocytic leukemia are associated with an increased risk for MCC (Becker et al., 2017). MCC carcinogenesis can be driven either by genomic integration of the Merkel cell polyomavirus (MCPyV) or chronic exposure to UV light (Becker et al., 2017).

MCC cells share morphological, immunohistological and ultrastructural features with Merkel cells, which serve as mechanoreceptors for light touch sensation and are among the few cell types in the skin displaying neuroendocrine features (Maricich et al., 2009). Both Merkel cells and MCC cells express neuroendocrine markers such as chromogranin-A, synaptophysin and cytokeratin 20 (CK20). However, there is no direct histogenetic link between Merkel cells and MCC (Becker et al., 2017).

Aberrant expression of microRNAs (miRNAs) in cancer is well established. miR-375 was recently identified among the most highly expressed miRNAs in classical MCC cell lines and tissues (Fan et al., 2018, Renwick et al., 2013, Xie et al., 2014). miR-375 was first identified as a pancreatic-islet miRNA regulating insulin secretion (Poy et al., 2004). While miR-375 expression is low in most cancer types (Yan et al., 2014), high expression of miR-375 is a characteristic of lung and small intestine cancers with neuroendocrine differentiation (Arvidsson et al., 2018, Miller et al., 2016, Nishikawa et al., 2011). In lung cancer, miR-375 is induced by the basic helix-loop-helix transcription factor Achaete-scute homolog 1 (ASCL1) (Nishikawa et al., 2011). However, ASCL1 is not present in MCC (Chteinberg et al., 2018), thus other helix-loop-helix transcription factors expressed in MCC such as Atonal

homolog 1 (ATOH1) may assume this task. ATOH1 is essential for Merkel cell development (Maksimovic et al., 2014, Ostrowski et al., 2015). It is reported to be down-regulated during MCC progression and thus has been suggested to act as a tumor suppressor (Bossuyt et al., 2009); however, a recent report demonstrated that expression of ATOH1 protein was increased in advanced MCCs (Gambichler et al., 2017). Moreover, only co-expression of the oncogenic MCPyV-derived T antigens together with ATOH1 resulted in the development of MCC-like tumors in mice (Verhaegen et al., 2017), thus supporting the notion that ATOH1 is relevant for MCC carcinogenesis. β-catenin, the key mediator of the canonical Wnt pathway, has been reported to be responsible for ATOH1 expression in neuroblastoma and neural progenitor cells (Shi et al., 2010); however, neither canonical nor non-canonical Wnt signaling seem to be involved in MCC carcinogenesis (Liu et al., 2007, Weeraratna et al., 2010). Hence, neither the induction nor the perpetuation of ATOH1 expression in MCC is fully understood.

RESULTS

ATOH1 expression correlates with miR-375 expression in MCC cells.

The high expression level of ATOH1 mRNA in MCC cells was confirmed in a large panel of MCC cell lines (n = 22; ref.(Fan et al., 2018)), whereas 13 non-MCC cell lines were all negative for its expression (**Fig. 1a**). MCC cell lines can be differentiated by their different growth patterns, i.e., classical MCC cell lines growing as spheroids or suspensions cells, whereas variant MCC cell lines show an adherent growth pattern. Of MCC cell lines, only classical MCC cell lines were characterized by high levels of ATOH1 mRNA. Consistent with this, protein expression of ATOH1 in classical MCC cell lines was confirmed by immunoblot (**Fig. 1b**). Neither in variant MCC cell lines, which are in contrast to classical

MCC cell lines as adherent cells, nor in squamous cell carcinoma (SCC) cell lines ATOH1 protein was detected. Similarly, ATOH1 mRNA expression was only detected in MCC tumor tissues but not in other non-MCC skin cancers (**Fig. 1c**). ATOH1 expression is likely to be modulated by differential DNA methylation in the ATOH1 promoter region (<1500 bps upstream of the start codon) as CpG islands were hypomethylated in classical MCC cell lines and tissues, whereas these regions were hypermethylated in variant MCC cell lines (**Fig. 1d**). Indeed, ATOH1 promoter methylation level negatively correlated with ATOH1 mRNA expression in MCC cell lines ($r = -0.86$, $p = 0.003$, **Fig. 1e**). It should be noted that expression of ATOH1 was not restricted to $MCPyV^+$ MCCs but was also present in $MCPyV^-$ classical MCC cell lines and tumor tissues.

miR-375 has been identified among the most abundant or highly expressed miRNAs in MCCs (Abraham et al., 2016, Fan et al., 2018, Renwick et al., 2013), but the fundamental molecular mechanism is unknown. In neuroendocrine lung cancer, miR-375 is induced by ASCL1, which is only weakly expressed in MCC cell lines and its expression did not correlate with that of miR-375 (**Suppl. Fig. S1a, b**). This finding was in line with reports that ASCL1 is absent or only occasionally present in MCC tumor tissues (Chteinberg et al., 2018, Ralston et al., 2008). Since ATOH1 is another member of the basic helix-loop-helix family of transcription factors, which like ASCL1 activates transcription by binding to E-boxes (5'-CANNTG-3'), and is highly expressed in MCC, we tested whether transcriptional activation of miR-375 in MCC is mediated by ATOH1. Indeed, when determining miR-375 expression level in a comparable MCC cell lines panel ($n = 21$), we observed a comparable expression pattern as for ATOH1 resulting in a significant correlation ($r = 0.88$, $p < 0.0001$; **Fig. 1f**). Moreover, the structure and methylation status of miR-375 promoter region also support the idea that miR-375 might be transcriptionally activated by ATOH1 in MCC (**Fig. 1g**). Besides the presence of E-boxes, an E47 binding site, which is required for E-box dependent

transcriptional activity of ATOH1 (Aguado-Llera et al., 2010), is present in the miR-375 promoter. More importantly, CpG islands around the E-boxes binding sites region are hypomethylated in classical MCC cells.

ATOH1 and miR-375 are not required for MCC cell proliferation

To test if ATOH1 induces miR-375 expression in MCC cells, a series of knockdown experiments were performed. Two predesigned dicer-substrate siRNAs (DsiRNAs) against ATOH1 (si-ATOH1-1 and si-ATOH1-2), which were transfected into the MCC cell lines WaGa and MKL1 by nuclear transfection, knocked down ATOH1 mRNA by approximately 50% in both cell lines (**Fig. 2a, Suppl. Fig. S1c**). Decreased ATOH1 protein expression was confirmed by immunoblot in WaGa cells (**Fig. 2b**). In line with our hypothesis, miR-375 expression was significantly downregulated by those DsiRNAs mediated ATOH1 knockdown (**Fig. 2c, Suppl. Fig. S1d**). Knockdown of ATOH1 did not alter cell viability and/or proliferation of transfected MCC cells (**Fig. 2d**). Consistent with this, inhibition of miR-375 by antagomir did not affect proliferation of WaGa and PeTa MCC cells (**Suppl. Fig. S2**). Taken together, despite the abundance of ATOH1 and miR-375 expression neither appears to be required for MCC cell proliferation.

ATOH1 induces miR-375 expression in variant MCC cells and skin fibroblasts

Next, we overexpressed ATOH1 in the ATOH1-negative variant MCC cell lines MCC13 and MCC26 as well as in primary skin fibroblasts (**Fig. 3a, b, e; Suppl. Fig. S3a, b**). Interestingly, upon overexpression of ATOH1 about 75% of cells changed their growth pattern from adherent to suspension within 48 hours after transfection (**Fig. 3c** top panels, **3f** top panels); ATOH1 overexpressing cells formed small cell clusters, resembling a neuroendocrine growth pattern. Moreover, ATOH1 mRNA expression was more pronounced in cells characterized by this neuroendocrine growth pattern as compared to those with

adherent growth (**Fig. 3a**). To confirm that these suspension cells are not merely presenting dying cells, a live/dead staining was performed by MitoView633 and NucView488 that detect catalytically active live cells (red) and caspase3-active dead cells (green), respectively (**Fig. 3c** bottom, **3f** bottom panels). To verify that ATOH1 stimulates the miR-375 promoter activity, a luciferase reporter construct containing no E-box, three E-boxes or mutated E-boxes was co-transfected with the ATOH1 expression vector pcDNA3-ATOH1-mCherry or the empty vector pcDNA3-mCherry into both MCC13 and MCC26 cells. Only the co-transfection of the reporter plasmid carrying E-boxes together with the ATOH1 expression vector resulted in a robust induction of luciferase activity indicating that the experimentally induced ATOH1 indeed binds to E-boxes (**Fig. 3d; Suppl. Fig. S3c**). We infer that in MCC cells, ATOH1 binds to the E-boxes within the miR-375 promoter and thereby induces its expression. Notably, in variant MCC cells after ATOH1 overexpression miR-375 was found significantly upregulated, and this miR-375 upregulation was pronounced in cells growing in suspension (**Fig. 3e; Suppl. Fig. S3d**). As described above, forced expression of ATOH1 in primary skin fibroblasts also altered their growth characteristics towards a neuroendocrine-like growth pattern (**Fig. 3f**). Furthermore, miR-375 expression was predominately induced in these suspension fibroblasts (**Fig. 3g**).

Ectopic expression of truncated MCPyV LTs in a fibroblast cell line induces both ATOH1 and miR-375 expression as well as a neuroendocrine-like growth pattern

To test if the MCPyV-encoded transforming early genes are able to trigger the ATOH1/miR-375 expression cascade, we expressed truncated MCPyV LTs, from which the sT coding sequence was removed, derived from the classical MCC cell lines MKL-1, MKL-2 and MS-1 in the fibroblast cell line MRC-5 (**Suppl. Fig. S4a**). As observed for ATOH1 overexpression in fibroblasts, a subset of transduced MRC-5 cells started to grow as suspension cells (**Fig. 4a**). Ectopic expression of these truncated MCPyV LTs induced endogenous ATOH1 and

miR-375 expression, which was more pronounced in MRC-5 cells growing in suspension (**Fig. 4b, c**), but not ASCL1 expression (data not shown). Meanwhile, truncated MCPyV LTs also boosted luciferase activity of a reporter plasmid carrying E-boxes (**Suppl. Fig. S4b**). In line with LT-induced ATOH1 expression, we observed in scRNAseq experiments that abundant LT and ATOH1 expression are apparently present in the same WaGa cells (**Fig. 4d-f**), and the observation was further confirmed by correlation analysis (**Suppl. Fig. S4c**, $r=0.62$, $p< 0.001$). In contrast, forced expression of MCPyV sT in MRC-5 cells did not significantly induce ATOH1 or miR-375 expression (**Suppl. Fig. S4d, e**), nor did it change the cell morphology and growth pattern (data not shown).

DISSCUSSION

The herein presented results demonstrate that MCPyV LT induced the expression of transcription factor ATOH1, which directly transactivates expression of miR-375, i.e. one of the most abundant microRNAs in this tumor. Notably, both LT-induced ATOH1 expression as well as subsequent ATOH1-mediated miR-375 induction appears to be boosted in MCC by hypomethylation of the respective promotor elements.

Development of MCC is frequently linked to the integration of MCPyV in the host genome, and it is known that several viruses manipulate the host's gene expression through epigenetic modifications (Engdahl et al., 2017, Kuss-Duerkop et al., 2018). For example, virally induced hypermethylation of immune-related genes is a common viral strategy to evade the hosts' immune responses (Kuss-Duerkop et al., 2018). However, viral infection can also decrease methylation levels to gain control of host gene expression (Kuss-Duerkop et al., 2018). Another example, human herpesvirus 6B (HHV-6B) infection leads to hypomethylation in telomere regions, which serve as HHB-6B integration sites as they are more accessible by

hypomethylation (Engdahl et al., 2017). In MCPyV positive MCC cells, LT of MCPyV might induce demethylation of the ATOH1 and miR-375 promoters, resulting in increased transcription of both ATOH1 and miR-375. Alternatively, LT may stimulate transcription of miR-375 by triggering ATOH1, or directly activate miR-375 expression. Thus, further investigation is required to elucidate the underlying mechanism.

However, strong expression of ATOH1 and miR-375 is also observed in MCPyV-negative classical MCC cell lines (but not in MCPyV-negative variant MCC cell lines). To this end, shared oncogenic pathways have been implicated in both virus-positive and UV-induced MCC (Gonzalez-Vela et al., 2017). Despite important genetic differences, both MCC etiologies exhibit nuclear accumulation of oncogenic transcription factors such as STAT3, which has been shown to induce ATOH1 expression (Zhang et al., 2012).

Our data indicate that ATOH1 is the major transcription factor for the observed miR-375 expression in MCC since forced ectopic expression of ATOH1 in primary skin fibroblasts as well as variant MCC cell lines induced miR-375 expression. Notably, ectopic ATOH1 expression in these adherently growing cell lines also changed their growth characteristics towards a neuroendocrine-like pattern, i.e., to suspension/ spheroids growth. Indeed, both induced ATOH1 and thereupon miR-375 expression was more pronounced in the proportion of suspension/ spheroids cells. This observation together with the notion that culture conditions of variant MCC cell lines enforcing a non-adherent growth, i.e., culture in ultra-low attachment plates or as hanging drops, did not change the expression of ATOH1 or miR-375 (data not shown), suggests that increased ATOH1/miR-375 expression is relevant for or may be even causing this neuroendocrine-like growth pattern. In line with this hypothesis, ATOH1 and miR-375 have both been reported to be strongly expressed in neuroendocrine cancers (Arvidsson et al., 2018, Flora et al., 2009, Northcott et al., 2009, Park et al., 2006).

Depending on the cellular context, ATOH1, *aka* Math1 and Hath1, may function both as an oncogene, e.g., in medulloblastoma (Briggs et al., 2008, Grausam et al., 2017) or as a tumor suppressor gene, e.g., in colon (Bossuyt et al., 2009, Fukushima et al., 2015), gastric (Han et al., 2015) and hepatocellular cancer (Gao et al., 2017). Despite its high expression in MCC tissues and in classical MCC cell lines (Gambichler et al., 2017), knockdown of ATOH1 did not affect cell viability or proliferation of MCC cells. Hence, we speculate that ATOH1 might rather be a lineage-dependency than a lineage-survival oncogene for MCC (Garraway and Sellers, 2006). However, other cell characteristics such as migration, invasion, or drug resistance after ATOH1 knockdown were not scrutinized. In line with the notion of ATOH1 functioning as lineage-dependency oncogene are recent reports demonstrating that ATOH1 is an essential co-factor for MCPyV T antigens induced carcinogenesis in mice (Verhaegen et al., 2017). In this regard, we observed that forced expression of truncated LTs derived from different MCC cell lines already induced expression of ATOH1 in the fibroblast cell line MRC-5. This induction was predominately observed in those cells which acquired a neuroendocrine growth pattern.

The possible role of miR-375 in MCC cells was also explored. In accordance with the report of Abraham et al. (Abraham et al., 2016), knockdown of miR-375 in classical MCC cell lines did neither alter their viability, proliferation rate, nor morphology (**Fig. S3** and data not show). However, miR-375 is an exosomal miRNA (Huang et al., 2015), which may promote carcinogenesis by paracrine effects such as polarizing the tumor microenvironment (Binenbaum et al., 2018, Cooks et al., 2018). To this end, we recently reported that conditioned medium from MCC cell culture contained miR-375, which was strongly enriched in the exosomal fraction (ref. (Fan et al., 2018), and data not shown).

In summary, we provide several lines of evidence suggesting that ATOH1 is induced by forced expression of truncated MCPyV LT and appears to act as a lineage-dependency

oncogene in MCC: either subsequent or direct overexpression of ATOH1 in variant MCC cell lines or fibroblasts induces a neuroendocrine growth pattern, which was paralleled by similar morphologic changes and miR-375 expression, a marker for the neuroendocrine phenotype of different cancers. Thus, MCPyV associated carcinogenesis is likely to induce the characteristic neuroendocrine features of MCC via induction of ATOH1.

MATERIAL AND METHODS

Cell lines and clinical samples

The MCC and non-MCC cell lines have been described in supplementary tables of our previous report (Fan et al., 2018). For tumor tissue analysis, formalin-fixed and paraffin-embedded (FFPE) samples of 23 MCCs and 48 melanomas were obtained from the department of Dermatology of University Hospital Essen were used.

Plasmids

pcDNA3.1-mCherry-ATOH1 and pTA-Luc plasmids were kindly provided by Tsuchiya's lab (Tokyo Medical and Dental University, Tokyo, Japan), pTA-3E-luc (3x E-boxes) and pTA-3EM-luc (3x mutated E-boxes) plasmids were generated from pTA-luc plasmids in our lab. pcDNA3.1 and pCMV-betaGAL plasmids were kindly provided by Jianfeng Huang (Medical University of Graz, Graz, Austria) and pLJM1-EGFP by David Sabatini (Addgene plasmid # 19319).

Quantitative real time polymerase chain reactions (qRT-PCR)

RNA was isolated using PeqGOLD total RNA Kit (VWR/ Peqlab, Erlangen, Germany) and transcribed into cDNA using the SuperScript IV reverse transcriptase according to the manufacturer's instructions. qRT-PCR was performed on the CFX Real-Time PCR system

(Bio-Rad Laboratories, Düsseldorf, Germany). HPRT or RPLP0 was used as endogenous control, ATOH1 or MCPyV LT mRNA expression was detected using SYBR green assays, and relative quantification was calculated by the $2^{-\Delta\Delta Cq}$ method using the respective untreated control or as indicated (Livak and Schmittgen, 2001). Primer sequences are given in supplementary table 1.

For miRNAs, Applied Biosystems™ TaqMan™ MicroRNA Assays (Thermo Fisher Scientific, Frankfurt, Germany) was performed according to the manufacturer's instructions. Pre-designed TaqMan microRNA assays for miR-375 (ID000564) were used. The quantification cycle threshold (Cq) values of target miRNAs were normalized to the small nucleolar RNA RNU6B (ID001093) and relative expression to the respective comparator was calculated using the $2^{-\Delta\Delta Cq}$ method.

Immunoblot

Cell lysates were generated as previously described (Skov et al., 2005). 4-12% bis-tris plus precast gels (Thermo Fisher Scientific) were applied for protein electrophoresis, samples were transferred to nitrocellulose membranes using iBlot dry blotting system (Thermo Fisher Scientific). Nitrocellulose membranes were blocked for one hour with 5% powdered skim milk in PBST (PBS supplemented with 0.05% Tween 20) and incubated overnight with a primary antibody. Primary antibodies used were anti-mCherry antibody (1:200; Novus Biologicals/ 1C51) for ATOH1-mCherry, anti-ATOH1 antibody (1:1000; LSBio/ B6529) and TUB 2.1 (1:2500; Sigma Aldrich) for β-tubulin. Next day, membranes were washed with PBST and incubated for one hour with the appropriate peroxidase-coupled secondary antibodies (Agilent Technologies, Ratingen, Germany), followed by visualization using the Plus-ECL chemiluminescence detection kit (Thermo Fisher Scientific).

DNA methylation microarray analysis

Infinium MethylationEPIC BeadChips (Illumina, Ense-Höingen, Germany) were used to measure DNA methylation level. Data analysis was performed in R version 3.4.4. Raw IDAT files were imported and further processed following the cross-package workflow by Maksimovic et al. (Maksimovic et al., 2016) incorporating the Bioconductor packages minfi (Aryee et al., 2014) and limma (Ritchie et al., 2015). Signals of the control probes and general quality control was assessed with the minfi qcReport function. Data were normalized using functional normalization (Fortin et al., 2014) implemented in minfi. Probes with a detection p-value above 0.01 in at least one sample was removed. For visualizing percentage of methylation, methylation levels were converted to beta-values ($\beta = M/(M+U)$), the ratio between methylated and the sum of methylated and unmethylated signal. For multidimensional scaling, methylation levels were converted to M-values ($M = \log_2(M/U)$), the logit transformation of the beta-values. No batch effects were detected with multidimensional scaling. Differentially methylated probes and differentially methylated regions were called as described (Maksimovic et al., 2016) and considered as significant if p-value <= 0.05. Annotation information provided by Illumina correspond to human genome (hg19) reference coordinates.

Transfection

For ATOH1 overexpression, luciferase assay and lentivirus production, Lipofectamine 3000 transfection reagent (Thermo Fisher Scientific) was used for transient transfection following the manufacturer's instructions. For ATOH1 and miR-375 knockdown, nuclear transfection was applied. $2x10^6$ MCC cells were seeded into a 6-well-plate 24 hours before transfection. 100 µl Nucleofector Kit V buffer (Lonza, Basel, Switzerland) mixed with 10 µl DsiRNA (IDT, Leuven, Belgium) or mirVana miRNA inhibitors (Thermo Fisher Scientific) (20 nM)

were added to the cells, electroporation was performed with program D-23 of Nucleofector 2B (Lonza) device.

Live/dead cell staining

Suspension growing cells were collected 36 hours after transfection or 5 days after the stably transduced MRC-5 cells were established, resuspended in 300 µl culture medium in cell imaging coverglass chambers (Eppendorf, Hamburg, Germany). NucView 488 and MitoView 633 apoptosis assay kit (Biotium, Fremont, United States) were applied to stain the cells according to instructions in the product protocol.

Luciferase assay

MCC13, MCC26 or MRC-5 cells ($1x10^5$) were seeded in a 12-well-plate 24 hours before transfection. pcDNA3.1, pcDNA3.1-mCherry-ATOH1, or MKL-1-LT, MKL-2-LT, MS-1-LT, or MCPyV-sT encoding plasmids were co-transfected with pTA-3E-luc or pTA-3EM-luc and Beta-Gal reporter plasmids using Lipofectamine 3000 reagent (Thermo Fisher Scientific). Transfection was performed according to the manufacturer's instructions. Cells were harvested 48 hours after transfection and ONE-Glo and Beta-Glo assay system (Promega, Wisconsin, United States) were applied to determine relative luciferase signals using FLUOstar Omega (BMG LABTECH, Ortenberg, Germany) following the manufacturer's instructions.

Lentivirus production and transduction

Truncated MCPyV large T antigens (LTs) derived from different MCC cell lines were cloned into pLJM1-EGFP plasmids. Lentivirus was produced in HEK293T cells by co-transfecting pLJM1-EGFP-LTs or pLJM1-EGFP plasmids with helper plasmids (pHCMV-G, pRSV rev and pMDLg/pRRE). Virus supernatants were harvested 48 hours after transfection and

filtered through 0.45 μm filters. For transduction, virus supernatants and 4μg/ml polybrene were added to the MRC-5 cells overnight, then cells were washed twice with culture medium. 1μg/ml puromycin was applied for 5 days to select transduced cells.

scRNAseq and gene expression analysis

Since WaGa cells grow in suspension no isolation step was required and cells were directly single cell barcoded using the 10x Genomics 3' Chromium v2.0 platform (Zheng et al., 2017) (10x Genomics, Leiden, Netherland). Library preparation was performed according to the 10x Genomics protocol and the library afterwards sequenced on an Illumina HiSeq 4000 (Illumina).

The Cell Ranger Single Cell Software Suite version 2.1.1 (http://10xgenomics.com/) was used with default settings to align cDNA reads to the hg19 human reference genome and the Merkel cell polyomavirus sequence (NC_010277.2). For quality control, cells with less than 1000 UMI counts, less than 200 genes or expressing more than 10% mitochondrial genes were removed from analyses leaving in total 4187 cells. The Seurat R package was used for normalization and biological analysis (Butler et al., 2018). Expression values in the count matrix were imputed after normalization using the software package MAGIC (van Dijk et al., 2018). Cell cycle scores were calculated using a list of cell cycle-related genes identified by Kowalczyk (Kowalczyk et al., 2015) and the Seurat "CellCycleScoring" function.

Data Availability Statement

Datasets related to methylation levels of ATOH1 and microRNA-375 in the article can be found at http://dx.doi.org/10.17632/zpbnvthp8b.1, an open-source online data repository hosted at Mendeley Data. Datasets of WaGa single cell RNA sequencing were uploaded to NCBI-GEO (GSE130346).

Statistical Analysis

Statistical analyses were performed using GraphPad Prism 6.0 Software (GraphPad Software Inc., San Diego, CA, USA). Experiments containing two groups were analyzed using Mann-Whitney U test. Experiments containing more than two groups were analyzed using Kruskal-Wallis test for unpaired non-parametric samples. R studio was applied in statistical analysis as indicated: ggpubr R package for correlation analysis. A p-value smaller than 0.05 was considered significant; the respective p-values are indicated in the figures as follows: *$p < 0.05$, **$p < 0.01$, ***$p < 0.001$.

CONFLICT OF INTEREST

J.C. Becker is receiving speaker's bureau honoraria from Amgen, Pfizer, MerckSerono and Sanofi, and is a paid consultant/advisory board member for eTheRNA, MerckSerono, Pfizer, 4SC and Sanofi. His group receives research grants from Bristol-Myers Squibb, Merck Serono, and Alcedis. None of the activities is related to the submitted work.

None of other authors indicated any potential conflicts of interest.

ACKNOWLEDGEMENTS

This work was part of the FP7 project IMMOMEC funded by the European Commission including funding for K. Fan. The authors like to thank Monique Verhaegen (University of Michigan) for the kind gift of classical MCPyV-negative MCC cell lines.

AUTHOR CONTRIBUTIONS

Conceptualization, D.S., J.C.B. and K.F.;

Methodology, C.R., D.S., J.C.B., and K.F.;

Formal analysis, C.R., D.S., J.C.B., J.G., and K.F.;

Investigation, C.R., K.F., and K.R.;

Resources, T.G., M.S., and U.M.;

Data curation, C.R., J.G., K.F. and T.G.;

Original Draft, J.C.B. and K.F.;

Review & Editing, C.R., D.S., J.C.B., J.G., K.F., K.R., T.G., M.S. and U.M.;

Visualization, D.S., J.G. and K.F.;

Supervision, D.S. and J.C.B;

Funding Acquisition, J.C.B.

REFERENCES

Abraham KJ, Zhang X, Vidal R, Pare GC, Feilotter HE, Tron VA. Roles for miR-375 in neuroendocrine differentiation and tumor suppression via Notch pathway suppression in Merkel cell carcinoma. Am J Pathol 2016;186:1025-35.

Aguado-Llera D, Goormaghtigh E, de Geest N, Quan XJ, Prieto A, Hassan BA, et al. The basic helix-loop-helix region of human neurogenin 1 is a monomeric natively unfolded protein which forms a "fuzzy" complex upon DNA binding. Biochemistry 2010;49:1577-89.

Arvidsson Y, Rehammar A, Bergström A, Andersson E, Altiparmak G, Swärd C, et al. miRNA profiling of small intestinal neuroendocrine tumors defines novel molecular subtypes and identifies miR-375 as a biomarker of patient survival. Mod Pathol 2018;31:1302-17.

Aryee MJ, Jaffe AE, Corrada-Bravo H, Ladd-Acosta C, Feinberg AP, Hansen KD, et al. Minfi: a flexible and comprehensive Bioconductor package for the analysis of Infinium DNA methylation microarrays. Bioinformatics 2014;30:1363-9.

Becker JC, Stang A, DeCaprio JA, Cerroni L, Lebbe C, Veness M, et al. Merkel cell carcinoma. Nat Rev Dis Primers 2017;3:17077.

Binenbaum Y, Fridman E, Yaari Z, Milman N, Schroeder A, Ben David G, et al. Transfer of miRNA in macrophage-derived exosomes induces drug resistance in pancreatic adenocarcinoma. Cancer Res 2018;78:5287-99.

Bossuyt W, Kazanjian A, De Geest N, Van Kelst S, De Hertogh G, Geboes K, et al. Atonal homolog 1 is a tumor suppressor gene. Plos Biol 2009;7:311-26.

Briggs KJ, Eberhart CG, Watkins DN. Just say no to ATOH: how HIC1 methylation might predispose medulloblastoma to lineage addiction. Cancer Res 2008;68:8654-6.

Butler A, Hoffman P, Smibert P, Papalexi E, Satija R. Integrating single-cell transcriptomic data across different conditions, technologies, and species. Nat Biotechnol 2018;36:411-20.

Chteinberg E, Sauer CM, Rennspiess D, Beumers L, Schiffelers L, Eben J, et al. Neuroendocrine key regulator gene expression in Merkel cell carcinoma. Neoplasia 2018;20:1227-35.

Cooks T, Pateras IS, Jenkins LM, Patel KM, Robles AI, Morris J, et al. Mutant p53 cancers reprogram macrophages to tumor supporting macrophages via exosomal miR-1246. Nat Commun 2018;9:771.

Engdahl E, Dunn N, Niehusmann P, Wideman S, Wipfler P, Becker AJ, et al. Human herpesvirus 6B induces hypomethylation on chromosome 17p13.3, correlating with increased gene expression and virus integration. J Virol 2017;91:e02105-16.

Fan K, Ritter C, Nghiem P, Blom A, Verhaegen ME, Dlugosz A, et al. Circulating cell-free miR-375 as surrogate marker of tumor burden in Merkel cell carcinoma. Clin Cancer Res 2018;24:5873-82.

Flora A, Klisch TJ, Schuster G, Zoghbi HY. Deletion of Atoh1 disrupts Sonic Hedgehog signaling in the developing cerebellum and prevents medulloblastoma. Science 2009;326:1424-7.

Fortin JP, Labbe A, Lemire M, Zanke BW, Hudson TJ, Fertig EJ, et al. Functional normalization of 450k methylation array data improves replication in large cancer studies. Genome Biol 2014;15:503.

Fukushima K, Tsuchiya K, Kano Y, Horita N, Hibiya S, Hayashi R, et al. Atonal homolog 1 protein stabilized by tumor necrosis factor alpha induces high malignant potential in colon cancer cell line. Cancer Sci 2015;106:1000-7.

Gambichler T, Mohtezebsade S, Wieland U, Silling S, Hoh AK, Dreissigacker M, et al. Prognostic relevance of high atonal homolog-1 expression in Merkel cell carcinoma. J Cancer Res Clin Oncol 2017;143:43-9.

Gao Q, Wang K, Chen K, Liang L, Zheng Y, Zhang Y, et al. HBx protein-mediated ATOH1 downregulation suppresses ARID2 expression and promotes hepatocellular carcinoma. Cancer Sci 2017;108:1328-37.

Garraway LA, Sellers WR. Lineage dependency and lineage-survival oncogenes in human cancer. Nat Rev Cancer 2006;6:593-602.

Gonzalez-Vela MDC, Curiel-Olmo S, Derdak S, Beltran S, Santibanez M, Martinez N, et al. Shared oncogenic pathways implicated in both virus-positive and UV-Induced Merkel cell carcinomas. J Invest Dermatol 2017;137:197-206.

Grausam KB, Dooyema SDR, Bihannic L, Premathilake H, Morrissy AS, Forget A, et al. ATOH1 promotes leptomeningeal dissemination and metastasis of Sonic Hedgehog subgroup medulloblastomas. Cancer Res 2017;77:3766-77.

Han ME, Baek SJ, Kim SY, Kang CD, Oh SO. ATOH1 can regulate the tumorigenicity of gastric cancer cells by inducing the differentiation of cancer stem cells. PLoS One 2015;10:e0126085.

Huang XY, Yuan TZ, Liang MH, Du MJ, Xia S, Dittmar R, et al. Exosomal miR-1290 and miR-375 as prognostic markers in castration-resistant prostate cancer. Eur Urol 2015;67:33-41.

Kaae J, Hansen AV, Biggar RJ, Boyd HA, Moore PS, Wohlfahrt J, et al. Merkel cell carcinoma: incidence, mortality, and risk of other cancers. J Natl Cancer Inst 2010;102:793-801.

Kowalczyk MS, Tirosh I, Heck D, Rao TN, Dixit A, Haas BJ, et al. Single-cell RNA-seq reveals changes in cell cycle and differentiation programs upon aging of hematopoietic stem cells. Genome Res 2015;25:1860-72.

Kuss-Duerkop SK, Westrich JA, Pyeon D. DNA tumor virus regulation of host DNA methylation and its implications for immune evasion and oncogenesis. Viruses 2018;10:pii: E82.

Liu S, Daa T, Kashima K, Kondoh Y, Yokoyama SJJocp. The Wnt signaling pathway is not implicated in tumorigenesis of Merkel cell carcinoma. J Cutan Pathol 2007;34:22-6.

Livak KJ, Schmittgen TDJm. Analysis of relative gene expression data using real-time quantitative PCR and the 2− ΔΔCT method. Methods 2001;25:402-8.

Maksimovic J, Phipson B, Oshlack A. A cross-package Bioconductor workflow for analysing methylation array data. F1000Res 2016;5:1281.

Maksimovic S, Nakatani M, Baba Y, Nelson AM, Marshall KL, Wellnitz SA, et al. Epidermal Merkel cells are mechanosensory cells that tune mammalian touch receptors. Nature 2014;509:617-21.

Maricich SM, Wellnitz SA, Nelson AM, Lesniak DR, Gerling GJ, Lumpkin EA, et al. Merkel cells are essential for light-touch responses. Science 2009;324:1580-2.

Miller HC, Frampton AE, Malczewska A, Ottaviani S, Stronach EA, Flora R, et al. MicroRNAs associated with small bowel neuroendocrine tumours and their metastases. Endocr Relat Cancer 2016;23:711-26.

Nishikawa E, Osada H, Okazaki Y, Arima C, Tomida S, Tatematsu Y, et al. miR-375 is activated by ASH1 and inhibits YAP1 in a lineage-dependent manner in lung cancer. Cancer Res 2011;71:6165-73.

Northcott PA, Fernandez-L A, Hagan JP, Ellison DW, Grajkowska W, Gillespie Y, et al. The miR-17/92 polycistron is up-regulated in Sonic Hedgehog-driven medulloblastomas

and induced by N-myc in Sonic Hedgehog-treated cerebellar neural precursors. Cancer Res 2009;69:3249-55.

Ostrowski SM, Wright MC, Bolock AM, Geng X, Maricich SM. Ectopic Atoh1 expression drives Merkel cell production in embryonic, postnatal and adult mouse epidermis. Development 2015;142:2533-44.

Park ET, Oh HK, Gum JR, Crawley SC, Kakar S, Engel J, et al. HATH1 expression in mucinous cancers of the colorectum and related lesions. Clin Cancer Res 2006;12:5403-10.

Poy MN, Eliasson L, Krutzfeldt J, Kuwajima S, Ma X, Macdonald PE, et al. A pancreatic islet-specific microRNA regulates insulin secretion. Nature 2004;432:226-30.

Ralston J, Chiriboga L, Nonaka D. MASH1: a useful marker in differentiating pulmonary small cell carcinoma from Merkel cell carcinoma. Mod Pathol 2008;21:1357-62.

Renwick N, Cekan P, Masry PA, McGeary SE, Miller JB, Hafner M, et al. Multicolor microRNA FISH effectively differentiates tumor types. J Clin Invest 2013;123:2694-702.

Ritchie ME, Phipson B, Wu D, Hu Y, Law CW, Shi W, et al. limma powers differential expression analyses for RNA-sequencing and microarray studies. Nucleic Acids Res 2015;43:e47.

Shi F, Cheng YF, Wang XL, Edge AS. Beta-catenin up-regulates Atoh1 expression in neural progenitor cells by interaction with an Atoh1 3' enhancer. J Biol Chem 2010;285:392-400.

Skov S, Pedersen MT, Andresen L, Straten PT, Woetmann A, Ødum NJCr. Cancer cells become susceptible to natural killer cell killing after exposure to histone deacetylase inhibitors due to glycogen synthase kinase-3–dependent expression of MHC class I–related chain A and B. Cancer Res 2005;65:11136-45.

Stang A, Becker JC, Nghiem P, Ferlay J. The association between geographic location and incidence of Merkel cell carcinoma in comparison to melanoma: An international assessment. Eur J Cancer 2018;94:47-60.

van Dijk D, Sharma R, Nainys J, Yim K, Kathail P, Carr AJ, et al. Recovering gene interactions from single-cell data using data diffusion. Cell 2018;174:716-29.

Verhaegen ME, Mangelberger D, Harms PW, Eberl M, Wilbert DM, Meireles J, et al. Merkel cell polyomavirus small T antigen initiates Merkel cell carcinoma-like tumor development in mice. Cancer Res 2017;77:3151-7.

Weeraratna AT, Houben R, O'Connell MP, Becker JC. Lack of Wnt5A expression in Merkel cell carcinoma. Arch Dermatol 2010;146:88-9.

Xie H, Lee L, Caramuta S, Hoog A, Browaldh N, Bjornhagen V, et al. MicroRNA expression patterns related to Merkel cell polyomavirus infection in human Merkel cell carcinoma. J Invest Dermatol 2014;134:507-17.

Yan JW, Lin JS, He XX. The emerging role of miR-375 in cancer. Int J Cancer 2014;135:1011-8.

Zhang X, Yang YT, Zhu R, Bai JY, Tian Y, Li XH, et al. H. pylori induces the expression of Hath1 in gastric epithelial cells via interleukin-8/STAT3 phosphorylation while suppressing Hes1. J Cell Biochem 2012;113:3740-51.

Zheng GX, Terry JM, Belgrader P, Ryvkin P, Bent ZW, Wilson R, et al. Massively parallel digital transcriptional profiling of single cells. Nat Commun 2017;8:14049.

FIGURE LEGENDS

Fig. 1: The highly expressed ATOH1 in MCC cell lines and tissues correlates with miR-375 expression

a: ATOH1 expression in 22 MCC cell lines (19 classical MCPyV positive [n=13, red] or negative [n=6, gray], and three variant MCC cell lines [blue] (details are described in Fan et al., 2018 (Table S1)) as well as 13 non-MCC skin cancer (melanoma, squamous cell carcinoma), lung cancer, kidney, and fibroblast cell lines (details are described in Fan et al., 2018 (Table S2)) was quantified by RT-qPCR in triplicates. The expression of ATOH1 was normalized to HPRT and is depicted relative to 293T cells as calculated by the $2^{-\Delta\Delta Cq}$ method. **b**: Immunoblot of ATOH1 in MCC and SCC cell lines, β-Tubulin served as endogenous control. **c**: ATOH1 expression in 40 non-MCC skin cancer tissue samples (35 melanoma [black] and 5 BCC [blue]) as well as 23 MCC tissue samples (14 MCPyV+ [red] and 9 MCPyV- [gray]) was determined by RT-qPCR in triplicate. The expression level of ATOH1 was normalized to HPRT and is depicted relative to one randomly selected melanoma sample as calculated by the $2^{-\Delta\Delta Cq}$ method. **d**: DNA methylation status of the CpG islands in ATOH1 promoter region (<1500bp before ATG) from classical MCC (green, n=9), variant MCC (purple, n=3) cell lines and MCC tissues (orange, n=3) was analyzed by Methylation EPIC Array. DNA methylation levels (β-values) were indicated as the line and shaded areas are defined by 95% confidence interval. **e**: Correlation analysis for ATOH1 promoter methylation level and ATOH1 mRNA expression level in MCC cell lines (5 MCPyV+ [red] and 4 MCPyV- [blue]) was performed in R using the "ggpubr" package. **f**: Correlation analysis for miR-375 expression level and ATOH1 mRNA expression level in MCC cell lines (13 MCPyV+ [red] and 8 MCPyV- [blue]) was performed in R using the "ggpubr" package. The expression of ATOH1 mRNA/ miR-375 was normalized to HPRT/ U6 and is depicted relative to 293T cells as calculated by the $2^{-\Delta\Delta Cq}$ method. **g**: Methylation patterns of the miR-375 gene

are depicted. The red bottom track refers to the miR-375 single exon gene structure annotation, whereby the arrows indicate the genomic orientation. The classical (green, n=9) and variant (blue, n=3) MCC tracks refer to the degree of methylation in percent over the classical and variant MCC cell lines. Each bar represents one single CpG site. The horizontal green block represents the location of a known CpG-islands (CpG rich regions). The 100 Vertebrates Conservation (Vert. Cons) track displays the DNA sequence conservation within vertebrates. A high degree of conservation outside of an exon in combination with a CpG-island suggests the possible presence of a promoter region.

Fig. 2: ATOH1 knockdown in WaGa cells downregulates miR-375 expression

a: ATOH1 expression in WaGa cells transfected with siRNAs against ATOH1 or control siRNA was quantified by RT-qPCR in triplicates. The expression of ATOH1 was normalized to HPRT and is depicted relative to control siRNA transfected cells as calculated by the $2^{-\Delta\Delta Cq}$ method (mean + SD). **b**: Immunoblot of ATOH1 in WaGa cells transfected with siRNAs against ATOH1 or control siRNA, β-Tubulin was used as endogenous control. **c**: miR-375 expression in WaGa cells transfected with siRNAs against ATOH1 or control siRNA was quantified by RT-qPCR in triplicates. The expression of miR-375 was normalized to U6 and is depicted relative to control siRNA transfected cells as calculated by the $2^{-\Delta\Delta Cq}$ method (mean + SD). **d**: 24 hours after nuclear transfection cells were seeded (1x 10^5 cells per well) and counted every two days. Values represent relative cell number to seeded transfected cells at day 0.

Fig. 3: Overexpressing ATOH1 in MCC13 cells induces miR-375 expression

a: ATOH1 expression in MCC13 cells transfected with ATOH1 expression plasmid or control plasmid and stratified by their growth pattern (A= adherent; S= suspension) was quantified by RT-qPCR in triplicates. The expression of ATOH1 was normalized to HPRT

and is depicted relative to untreated cells as calculated by the $2^{-\Delta\Delta Cq}$ method (mean + SD). **b**: Immunoblot of ATOH1 in MCC13 cells overexpressing ATOH1 (cells growing adherent or in suspension were separated before analysis); beta-Tubulin served as endogenous control. **c**: upper row- morphology change of MCC13 cells overexpressing ATOH1; lower row- floating cells were stained with NucView® 488 and MitoView™ 633 apoptosis assay kit. Living cells were stained with red while dead/apoptotic cells were stained with green. Scale bar = 50 µM. **d**: Luciferase reporter assay to determine E-box activity. MCC13 were co-transfected with pTA-luc, pTA-3E-luc or pTA-3EM-luc, pCMV-betaGAL as exogenous control, and either control vector or ATOH1 vector. Values represent luciferase activity relative to cells transfected with control plasmid. **e**: miR-375 expression in MCC13 cells transfected with ATOH1 expression plasmid or control plasmid was quantified by RT-qPCR in triplicates. The expression of miR-375 was normalized to U6 and is depicted relative to untreated cells as calculated by the $2^{-\Delta\Delta Cq}$ method (mean + SD). **f**: Upper row- morphology change of primary skin fibroblasts (Fibro 1.7) overexpressing ATOH1; lower row- floating cells stained with NucView® 488 and MitoView™ 633 apoptosis assay kit. Living cells were stained with red and dead/apoptotic cells were stained with green. Scale bar = 50 µM. **g**: miR-375 expression in primary skin fibroblasts (Fibro 1.2 and Fibro 1.7) transfected with ATOH1 expression plasmid or control plasmid was quantified by RT-qPCR in triplicates. The expression of miR-375 was normalized to U6 and is depicted relative to control cells as calculated by the 2-ΔΔCq method (mean + SD).

Fig. 4: Overexpressed truncated MCPyV LTAs induces ATOH1 expression as well as miR-375 expression in MRC-5 cells

a: Upper row- morphology changes of MRC-5 cells transduced with different truncated MCPyV LTAs derived from MCC cell lines; lower row- floating growing cells stained with NucView® 488 and MitoView™ 633 apoptosis assay kit. Living cells were stained with red

and dead/apoptotic cells were stained with green. Scale bar = 50 µM. **b**: ATOH1 expression in MRC-5 cells (adherent and suspension cells were analyzed separately) transduced with different truncated MCPyV LTAs expression constructs quantified by RT-qPCR in triplicates. The expression of ATOH1 was normalized to RPLP0 and is depicted relative to EGFP cells as calculated by the $2^{-\Delta\Delta Cq}$ method (mean + SD). **c**: miR-375 expression in MRC-5 cells expressing different truncated MCPyV LTAs was quantified by RT-qPCR in triplicates. The expression of miR-375 was normalized to U6 and is depicted relative to EGFP cells as calculated by the $2^{-\Delta\Delta Cq}$ method (mean + SD). **d-f**: Principle component analysis (PCA) of single cell sequenced WaGa cells. **d**: PCA based exclusively on cell cycle marker genes, cells are colored with respect to their cell cycle. **e** and **f**: Expression level of MCPyV LTA mRNA (**e**) and ATOH1 mRNA (**f**) in WaGa cells in principle component reduced space. Expression values were imputed using the software MAGIC to compensate for dropouts typical for 10x Genomics scRNA-seq.

Figure 1

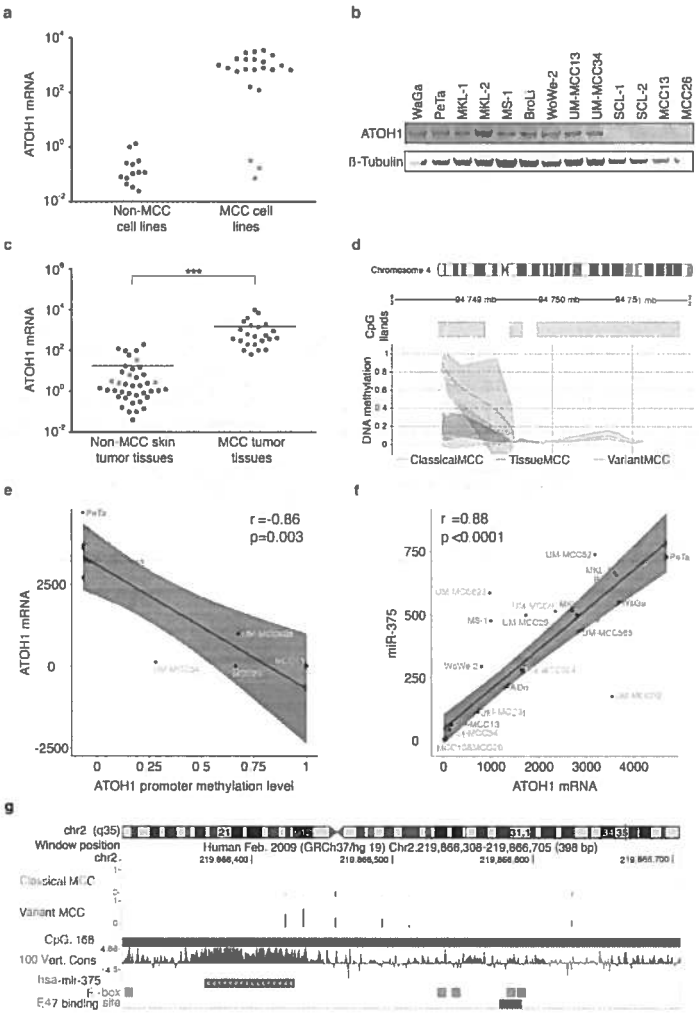
a
ATOH1 mRNA
Non-MCC cell lines
MCC cell lines
b
WaGa
PeTa
MKL-1
MKL-2
MS-1
BroLi
WoWe-2
UM-MCC13
UM-MCC34
SCL-1
SCL-2
MCC13
MCC26
ATOH1
ß-Tubulin
c
***
ATOH1 mRNA
Non-MCC skin tumor tissues
MCC tumor tissues
d
Chromosome 4
CpG Ilands
DNA methylation
ClassicalMCC
TissueMCC
VariantMCC
e
r =-0.86
p=0.003
ATOH1 mRNA
ATOH1 promoter methylation level
f
r =0.88
p <0.0001
miR-375
ATOH1 mRNA
g
chr2 (q35)
Window position
Human Feb. 2009 (GRCh37/hg 19) Chr2:219,866,308-219,866,705 (398 bp)
Classical MCC
Variant MCC
CpG. 168
100 Vert. Cons
hsa-mir-375
E47 binding site

Figure 2

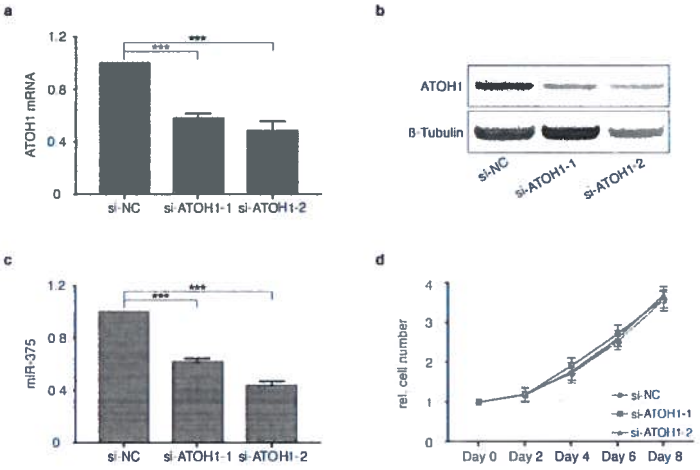
a
ATOH1 mRNA
1.2
0.8
0.4
0
***
***
si-NC
si-ATOH1-1
si-ATOH1-2
b
ATOH1
β-Tubulin
si-NC
si-ATOH1-1
si-ATOH1-2
c
miR-375
1.2
0.8
0.4
0
***
***
si-NC
si-ATOH1-1
si-ATOH1-2
d
rel. cell number
4
3
2
1
0
si-NC
si-ATOH1-1
si-ATOH1-2
Day 0
Day 2
Day 4
Day 6
Day 8

Figure 3

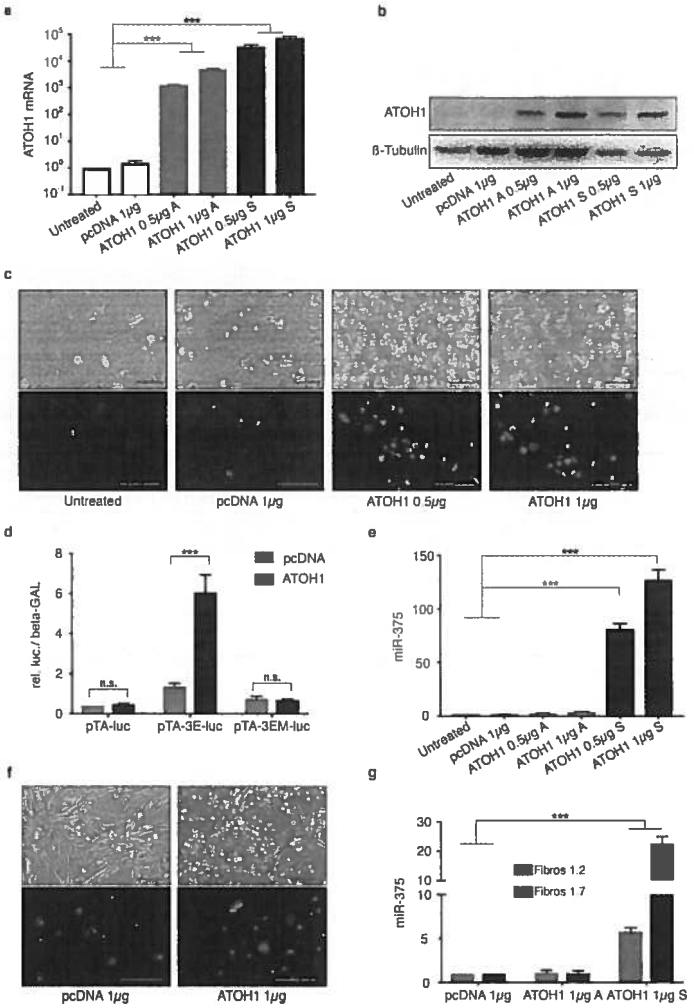
a
ATOH1 mRNA
Untreated
pcDNA 1µg
ATOH1 0.5µg A
ATOH1 1µg A
ATOH1 0.5µg S
ATOH1 1µg S
b
ATOH1
ß-Tubulin
Untreated
pcDNA 1µg
ATOH1 A 0.5µg
ATOH1 A 1µg
ATOH1 S 0.5µg
ATOH1 S 1µg
c
Untreated
pcDNA 1µg
ATOH1 0.5µg
ATOH1 1µg
d
rel. luc./ beta-GAL
pcDNA
ATOH1
n.s.
pTA-luc
pTA-3E-luc
pTA-3EM-luc
e
miR-375
Untreated
pcDNA 1µg
ATOH1 0.5µg A
ATOH1 1µg A
ATOH1 0.5µg S
ATOH1 1µg S
f
pcDNA 1µg
ATOH1 1µg
g
miR-375
Fibros 1.2
Fibros 1.7
pcDNA 1µg
ATOH1 1µg A
ATOH1 1µg S

Figure 4

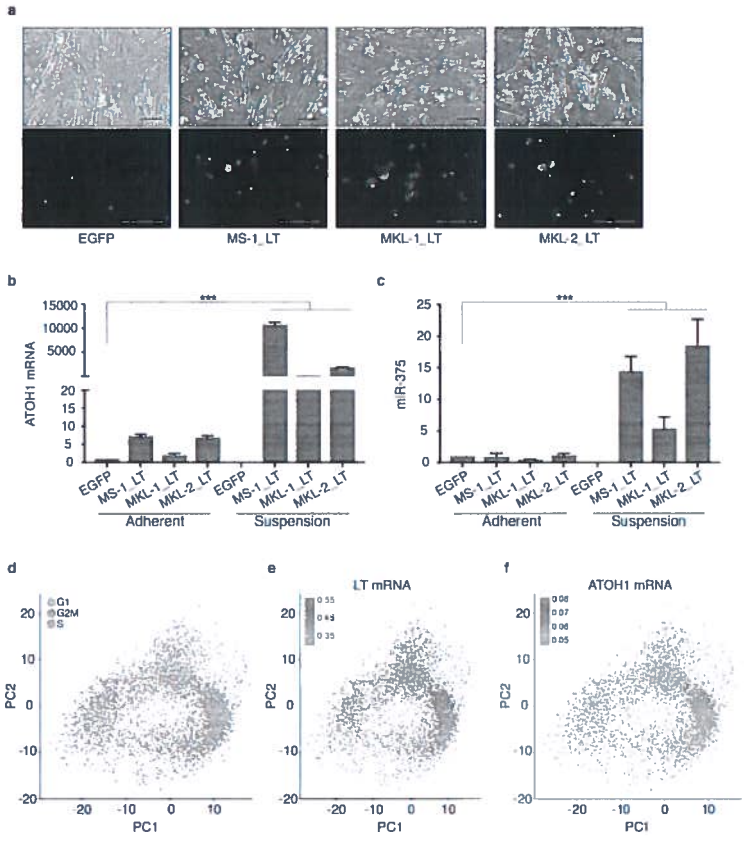
a
EGFP
MS-1_LT
MKL-1_LT
MKL-2_LT
b
ATOH1 mRNA
15000
10000
5000
20
15
10
5
0
***
EGFP
MS-1_LT
MKL-1_LT
MKL-2_LT
Adherent
Suspension
c
miR-375
25
20
15
10
5
0
***
Adherent
Suspension
d
G1
G2M
S
PC2
PC1
e
LT mRNA
PC2
PC1
f
ATOH1 mRNA
PC2
PC1

Supplementary table 1: Primers used for qRT-PCR

ASCL1_fw	CCCAAGCAAGTCAAGCGACA
ASCL1_rv	AAGCCGCTGAAGTTGAGCC
ATOH1_fw	TGAAGGAGTTGGGAGACCAC
ATOH1_rv	GTAGACGGGATGCTCTCTCG
MCPyV-LTA_fw	CTCGTCAACCTCATCAAAC
MCPyV-LTA_rv	GGAGCAAATTCCAGCAAA
HPRT_fw	GTCGTGATTAGTGATGATG
HPRT_rv	GTTCAGTCCTGTCCATAA
RPLP0_fw	CCATCAGCACCACAGCCTTA
RPLP0_rv	GGCGACCTGGAAGTCCAACT
RPLP0_TP	YY-ATCTGCTGCATCTGCTTGGAGCCCA-BHQ1

Figure S1

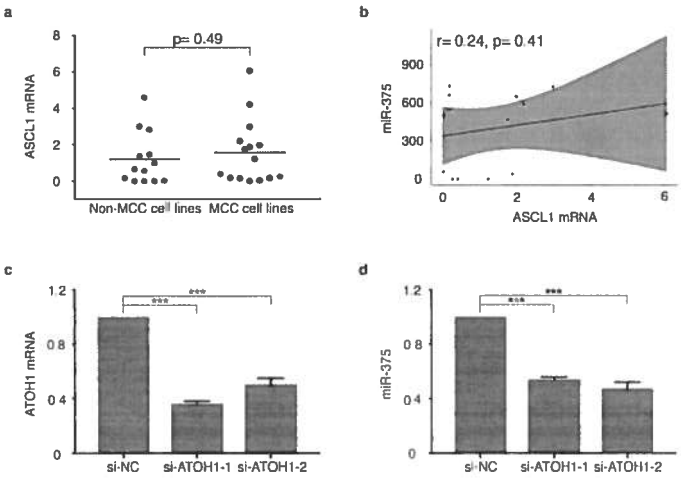

Figure S2

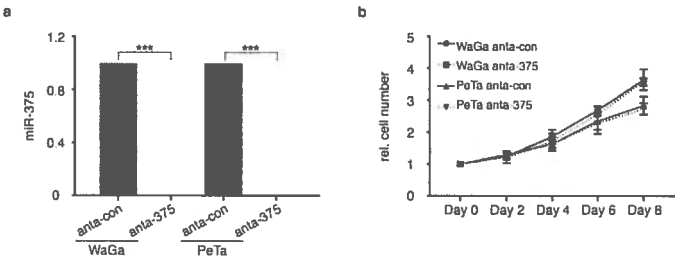
a
1.2
0.8
0.4
0
miR-375
***
***
anta-con
anta-375
anta-con
anta-375
WaGa
PeTa
b
5
4
3
2
1
0
rel. cell number
WaGa anta-con
WaGa anta-375
PeTa anta-con
PeTa anta-375
Day 0
Day 2
Day 4
Day 6
Day 8

Figure S3

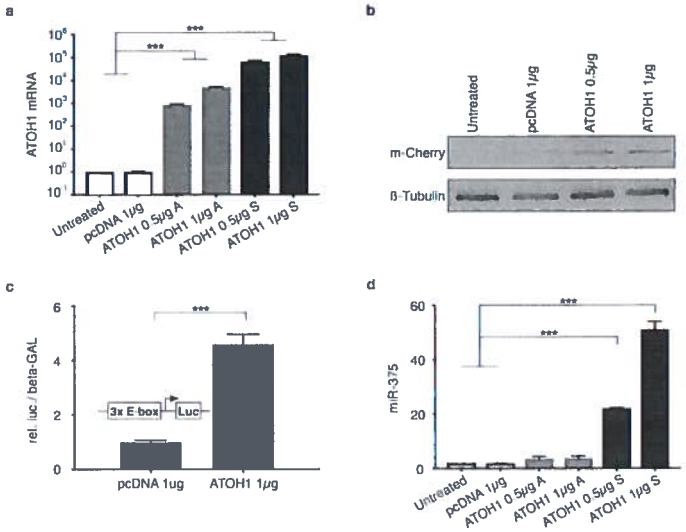

Figure S4

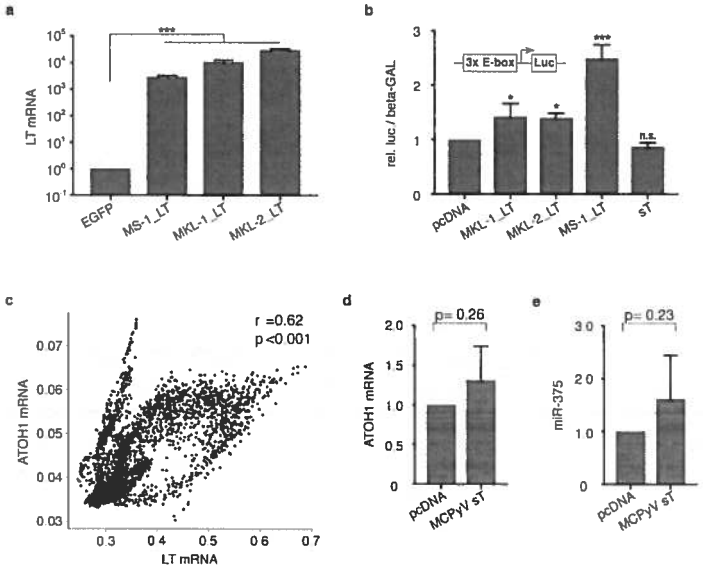
a
LT mRNA
***
EGFP
MS-1_LT
MKL-1_LT
MKL-2_LT
b
rel. luc./beta-GAL
3x E-box
Luc
*
*
***
n.s.
pcDNA
MKL-1_LT
MKL-2_LT
MS-1_LT
sT
c
r =0.62
p <0.001
ATOH1 mRNA
LT mRNA
d
p= 0.26
ATOH1 mRNA
pcDNA
MCPyV sT
e
p= 0.23
miR-375
pcDNA
MCPyV sT